⁸Cloud Radiative Feedbacks and El Niño-Southern Oscillation [®]

ELEANOR A. MIDDLEMAS AND AMY C. CLEMENT

Rosenstiel School of Marine and Atmospheric Sciences, University of Miami, Miami, Florida

BRIAN MEDEIROS

National Center for Atmospheric Research, Boulder, Colorado

BEN KIRTMAN

Rosenstiel School of Marine and Atmospheric Sciences, University of Miami, Miami, Florida

(Manuscript received 7 December 2018, in final form 30 April 2019)

ABSTRACT

Cloud radiative feedbacks are disabled via "cloud-locking" in the Community Earth System Model, version 1.2 (CESM1.2), to result in a shift in El Niño–Southern Oscillation (ENSO) periodicity from 2–7 years to decadal time scales. We hypothesize that cloud radiative feedbacks may impact the periodicity in three ways: by 1) modulating heat flux locally into the equatorial Pacific subsurface through negative shortwave cloud feedback on sea surface temperature anomalies (SSTA), 2) damping the persistence of subtropical southeast Pacific SSTA such that the South Pacific meridional mode impacts the duration of ENSO events, or 3) controlling the meridional width of off-equatorial westerly winds, which impacts the periodicity of ENSO by initiating longer Rossby waves. The result of cloud-locking in CESM1.2 contrasts that of another study, which found that cloud-locking in a different global climate model led to decreased ENSO magnitude across all time scales due to a lack of positive longwave feedback on the anomalous Walker circulation. CESM1.2 contains this positive longwave feedback on the anomalous Walker circulation, but either its influence on the surface is decoupled from ocean dynamics or the feedback is only active on interannual time scales. The roles of cloud radiative feedbacks in ENSO in other global climate models are additionally considered. In particular, it is shown that one cannot predict the role of cloud radiative feedbacks in ENSO through a multimodel diagnostic analysis. Instead, they must be directly altered.

1. Introduction

Cloud radiative feedbacks, or the interaction between cloud radiative effects and atmospheric circulation and sea surface temperature (SST), are a major source of uncertainty among atmospheric feedbacks related to El Niño–Southern Oscillation (ENSO) (Lloyd et al. 2009, 2011, 2012; Bellenger et al. 2014; Rädel et al. 2016).

Oenotes content that is immediately available upon publication as open access.

© Supplemental information related to this paper is available at the Journals Online website: https://doi.org/10.1175/JCLI-D-18-0842.s1.

Corresponding author: Eleanor A. Middlemas, e.middlemas@rsmas.miami.edu

Isolating the impact of these cloud feedbacks on the evolution of El Niño and La Niña events remains a challenge. Warm SST anomalies (SSTA) during El Niño events are accompanied by westerly wind anomalies, a deepening thermocline through the Bjerknes feedback, and an eastward shift in the Walker circulation. The opposite occurs during La Niña events. Cloud radiative feedbacks may influence both the anomalous Walker circulation as well as thermodynamic damping of ENSO SSTA variability in the central tropical Pacific. The degree of thermodynamic damping is determined by the magnitude of the net surface heat flux feedback, which is defined by the sum of the shortwave (SW), latent heat flux, sensible heat flux, and longwave (LW) feedbacks (Lloyd et al. 2009, 2011). Considering the sheer complexity of ENSO events, it is no surprise that isolating the impact of cloud radiative feedbacks on ENSO poses a challenge. In this study, we pinpoint their precise

DOI: 10.1175/JCLI-D-18-0842.1

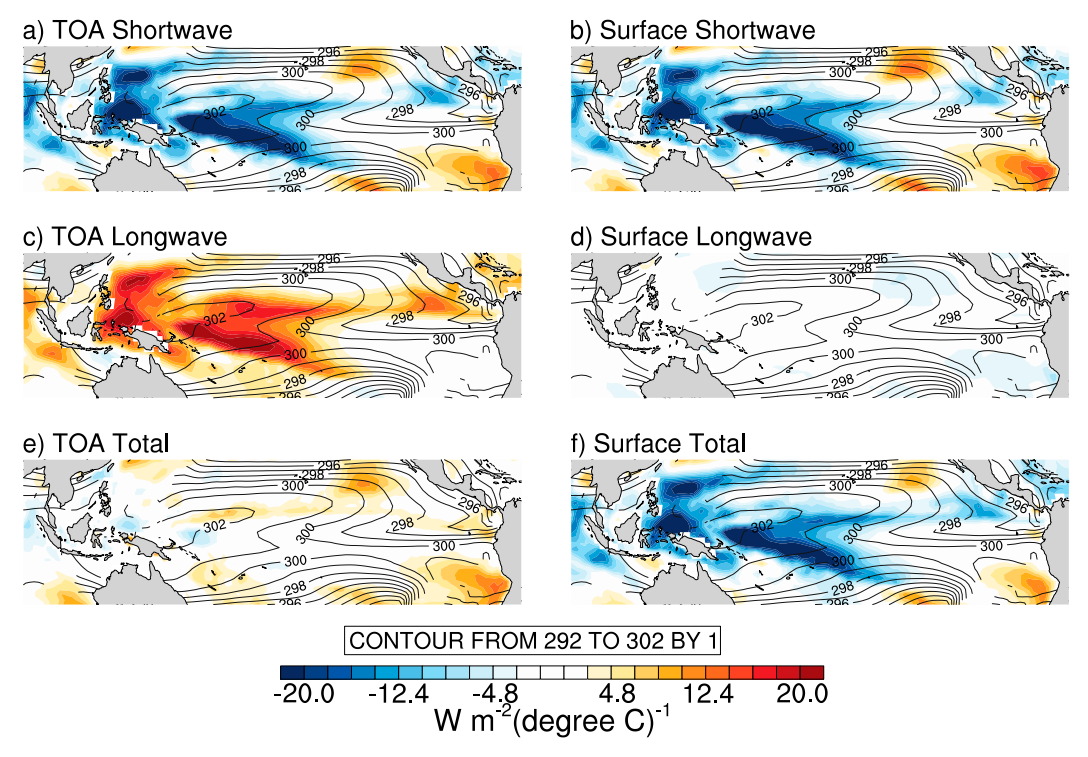


FIG. 1. Cloud radiative feedback from observations over the period March 2000–February 2017. Cloud radiative feedback is calculated as the pointwise regression of cloud radiative forcing onto sea surface temperature (SST) anomalies (colors) at (left) the top of atmosphere (TOA) and (right) the surface. Climatological SST is overlaid (contours). Cloud radiative forcing is taken from the CERES-EBAF-v4 monthly flux dataset. SST is taken from NOAA ERSSTv5. SST has climatology from 1971 to 2000 as well as the annual mean value removed prior to cloud radiative feedback calculation.

role by prescribing cloud radiative effects (or "cloud-locking") in a fully coupled global climate model.

Classical conceptual models attempting to explain the oscillatory nature and the period of ENSO include the delayed oscillator theory (Suarez and Schopf 1988; Battisti and Hirst 1989) the recharge/discharge oscillator (Jin 1997), oceanic Kelvin waves forced by westerly wind anomalies (Weisberg and Wang 1997), and the ocean advective–reflective model (Picaut et al. 1997). None of these conceptual models explicitly includes the role of cloud radiative feedbacks in determining the periodicity, but instead considers only surface winds, thermodynamic damping, and ocean dynamics. However, cloud feedbacks are a potentially important part of surface heat flux damping, and hence may play a role as well in setting the period of ENSO.

To assess the impact of prescribing cloud radiative effects on ENSO, consider the mechanisms of cloud radiative feedbacks. Warm sea surface temperature anomalies during El Niño events encourage deep moist convection that produces high-level ($p < 400 \,\mathrm{hPa}$) anvil clouds in the western-central Pacific. These anvils reflect incident shortwave radiation, cooling the surface and

creating a negative SW feedback on SSTA at the surface, as shown in observations in Fig. 1b. Deep convective anvils also absorb upwelling longwave radiation, emitted at relatively cold upper tropospheric temperature, thus reducing outgoing longwave radiation (OLR) and further warming the atmosphere. This positive LW feedback on SSTA is evident from the top-of-atmosphere perspective in observations (Fig. 1c). Over the regions of warm SSTA, SW and LW feedbacks on SSTA nearly cancel at the top of the atmosphere (TOA) (Fig. 1e), but SW dominates at the surface due to the small absorption of SW by the atmosphere (Figs. 1a,b,f). Over cool SSTA found in the far eastern Pacific or during La Niña events, one or more of the following occur: atmospheric subsidence, increased lower atmospheric stability, or a sharp temperature inversion in the lower atmosphere—all of which encourage the formation of optically thick low-level stratocumulus clouds (Klein and Hartmann 1993; Norris 1998; Myers and Norris 2015). These clouds block incident radiation and further cool the underlying SST, thus creating a positive SW feedback on SSTA (Fig. 1b) (Philander et al. 1996; Clement et al. 2009; Dommenget 2010; Lloyd et al. 2011; Bellomo et al. 2014; Burgman et al. 2017).

Changes in longwave radiation due to clouds may also interact with convection and the Walker circulation as a result. Deep convective anvils are opaque in the infrared and trap much of the OLR-in contrast to low-level clouds that emit LW at a temperature similar to the surface. The trapping of OLR by deep convective anvils enhances atmospheric instability and strengthens convection as a result (Slingo and Slingo 1988, 1991; Randall et al. 1989; Bretherton and Sobel 2002). Using the MPI-ESM-LR global climate model with cloud radiative feedbacks artificially removed, Rädel et al. (2016) found that, by disabling cloud radiative feedbacks, positive longwave feedback on SSTA and on atmospheric circulation results in a stronger anomalous Walker circulation and stronger ENSO SSTA variability, while SW feedback plays a much smaller role. Considering the large spread in equatorial Pacific cloud feedbacks and ENSO strength across CMIP5 models, this balance of SW and LW cloud radiative feedbacks is likely model-specific. In fact, Bellenger et al. (2014) showed that MPI-ESM-LR produces more subsidence or weaker convection than observations in the tropical Pacific, which ultimately results in ENSO events with smaller magnitude due to an unrealistic SW cloud radiative feedback. This implies that a model with a more realistic SW feedback (and larger ENSO events) will likely find a different balance of radiative feedbacks. We conduct experiments similar to those of as Rädel et al. (2016) in CESM1.2 to find that the role of SW feedbacks is critical for ENSO evolution.

2. Methodology: Cloud-locking and diagnostics of ENSO and cloud radiative feedback

The locking of model fields such as water vapor, clouds, or albedo has been implemented in various models since the 1980s, typically to measure the associated feedback in terms of climate response to changes in external forcing (Wetherald and Manabe 1980, 1988; Zhang et al. 2010; Langen et al. 2012; Ceppi and Shepherd 2017; Mauritsen et al. 2013; Voigt and Shaw 2015; Trossman et al. 2016). The goal of the aforementioned studies is to assess the role of cloud feedbacks in climate sensitivity, so cloud fields from an experiment with one level of greenhouse gas forcing are prescribed in another experiment with a different level of greenhouse gas forcing. Instead, we are interested in the contribution of cloud feedback to internal variability of the climate system, ENSO in particular, so we implement cloud-locking using two experiments with identical forcing. The clouds are extracted from an experiment with constant preindustrial forcing and are prescribed in an experiment that also has preindustrial control forcing. Cloud-locking isolates the impact of cloud feedback because cloud feedbacks are active in the control simulation and inactive in the cloud-locked experiment. In the control simulation, CRE forces, as well as responds to, anomalous circulation and sea surface temperature, whereas in the cloud-locked experiment CRE is prescribed. CRE varies independently from the climate of the cloud-locked experiment.

We use the Community Earth System Model, version 1.2 (CESM1.2) (Hurrell et al. 2013). All simulations presented in this study are run at a horizontal resolution of 0.9° latitude \times 1.25° longitude. We prescribe clouds in the radiation model of the atmospheric component of CESM1.2, the Community Atmospheric Model, version 5 (CAM5), and in this way the cloud radiative effect (CRE) is decoupled from atmospheric circulation and SST. Cloud-locking is executed as follows: first, clouds are extracted from the control simulation, which is the long preindustrial control experiment that is part of the CESM Large Ensemble Community Project (Kay et al. 2015). To extract the cloud, we branch off year 1366, an ENSOneutral year, and save one year of instantaneous 3D cloud fields before the radiation module is called. The extracted cloud fields include eight macro- and microphysical cloud parameters: cloud amount; effective diameters of rain, ice, and snow; in-cloud liquid water path; in-cloud ice water path; and two microphysical parameters, μ and λ , describing the width and height of the distribution of water droplets in a given grid box. We subsequently perform the cloud-locked experiment by reading these eight parameters every 2h and using them as input to the radiative transfer calculation. Additional experiments showed that radiative balance is insensitive to prescribing more frequent cloud fields (not shown); the model calls the radiative transfer calculation every hour, while the rest of the physics is calculated every 0.5 h (and the dynamics is subcycled with a 6-min time step). The year of cloud parameter data is repeated in order to remove interannual climate variability from cloud fields while maintaining the seasonal cycle. Thus, our experiments are free-running and hence simulating climate variability, but the radiative calculations use cloud parameters from the same year repeatedly.

Cloud-locking in CESM1.2 results in a small global-mean cooling (see Fig. S1 in the online supplemental material) that we assert is insignificant for the objective of our study. Climate drift due to cloud-locking has been reported in other variable-locking studies and is due to the loss of spatiotemporal correlation between cloud moisture and temperature anomalies (Schneider et al. 1999; Langen et al. 2012; Mauritsen et al. 2013). Since dynamics are calculated with prognostic clouds and radiation is calculated with prescribed cloud, unphysical synoptic situations can occur. For example, the prescribed

TABLE 1. CMIP5 models and their simulation length used in the multimodel analysis in sections 3f and 3g. All experiments utilize preindustrial control forcing.

Model name	Length (years)
ACCESS1.0	250
BNU-ESM	558
CanESM2	996
CCSM4	314
CESM1.2	500
CNRM-CM5	529
GFDL CM3	500
GFDL-ESM2G	500
GFDL-ESM2M	500
GISS-E2-H	480
HadGEM2-ES	489
INM-CM4	500
IPSL-CM5A-LR	1000
IPSL-CM5A-MR	300
MIROC5	529
MIROC-ESM	531
MPI-ESM-LR	186
MPI-ESM-P	150
MRI-CGCM3	339
NorESM1-ME	252
NorESM1-M	501

cloud may lead to a nonzero CRE in a grid box that is dynamically cloud-free. In our experiment, the global mean temperature of the cloud-locked experiment drifts to about ~1°C cooler than the control run over the course of 400 years (Fig. S1). Most of the adjustment occurs within the first 30 years (Fig. S1), so only the last 370 years are analyzed. The cooling is most prominent in polar regions (Fig. S2) whereas the changes in the tropics are small and insignificant compared to the changes in variance due to cloud-locking (Fig. 4).

In addition, we compare CESM1.2's cloud radiative feedback on ENSO to that in observations and 21 models from phase 5 of the Climate Model Intercomparison Project (CMIP5) (Taylor et al. 2012) listed in Table 1. The observations used are sea surface temperature from the National Atmospheric and Ocean Administration (NOAA) Extended Reconstructed Sea Surface Temperature, version 5 (ERSSTv5) (Huang et al. 2017) and CRE from the Clouds and the Earth's Radiant Energy System Energy Balanced and Filled dataset, version 4 (CERES-EBAF-v4) (Loeb et al. 2018). The observations overlap during the interval from March 2000 through February 2017. All of the CMIP5 experiments analyzed are forced with constant preindustrial greenhouse gas levels and vary in length from 150 to 1000 years (Table 1). CRE is calculated from CMIP5 data as shortwave (positive down) minus longwave (positive up) total-sky fluxes minus the corresponding clear-sky fluxes: $CRE = (SW_{\perp} - LW_{\uparrow})$ -

 $(SW_{clearsky,\downarrow} - LW_{clearsky,\uparrow})$. We then calculate cloud radiative feedback (CRFB) as CRE (with the mean removed) regressed on local SST anomalies (with seasonal cycle and mean removed):

$$CRFB = \frac{dCRE}{dT} = \frac{dCRE_{SW}}{dT} + \frac{dCRE_{LW}}{dT},$$

which may be split up further into SW and LW components and may be considered at either TOA or the surface:

$$CRFB_{TOA} = CRFB_{SWTOA} + CRFB_{LWTOA}$$

or

$$CRFB_{surf} = CRFB_{SW,surf} + CRFB_{LW,surf}$$

Both surface and TOA feedbacks are disabled by the cloud-locking experiments, but we refer to one or the other when discussing physical mechanisms. When we discuss the shortwave component (SW CRFB), we refer to the surface feedback (Fig. 1b) because the impact of shortwave feedback on water vapor and atmosphere is small in the TOA feedback (Figs. 1a,b). For the longwave feedback (LW CRFB), we refer to the TOA component (Fig. 1c) due to the impact of positive longwave feedback on atmospheric temperature, which influences the surface temperature indirectly through circulation and surface winds (Rädel et al. 2016).

We use the Niño-3.4 index extensively in this study; the results are similar for other Niño indices. The Niño-3.4 index is defined as the 1-2-1 smoothed SST anomalies over 5°S to 5°N and 120°-170°W. In this study, "anomalies" refers to fields with the seasonal cycle removed. El Niño and La Niña composites are made by averaging across El Niño or La Niña events. El Niño events are defined as Niño-3.4 anomalies that exceed one standard deviation σ for five consecutive months or longer. This definition is based on the NOAA operational forecast definition. To prevent overlap, we select the largest event between two that occur within 3 years of each other. La Niñas are selected in a similar fashion except that they are based on Niño-3.4 anomalies less than -1σ . Defining El Niño or La Niña events differently may result in a different number of events, but the differences between the control and cloud-locking experiment remains the same.

We calculate CRFB as the regression of CRE onto the Niño-3.4 index. An average of the pointwise regression of CRE on local SST in the Niño-3.4 region yields similar values as those regressed on Niño-3.4 index. In observations, the seasonal cycle is removed from the Niño-3.4 index before calculating the CRFB. Calculating CRFB as the regression of CRE onto SST has been

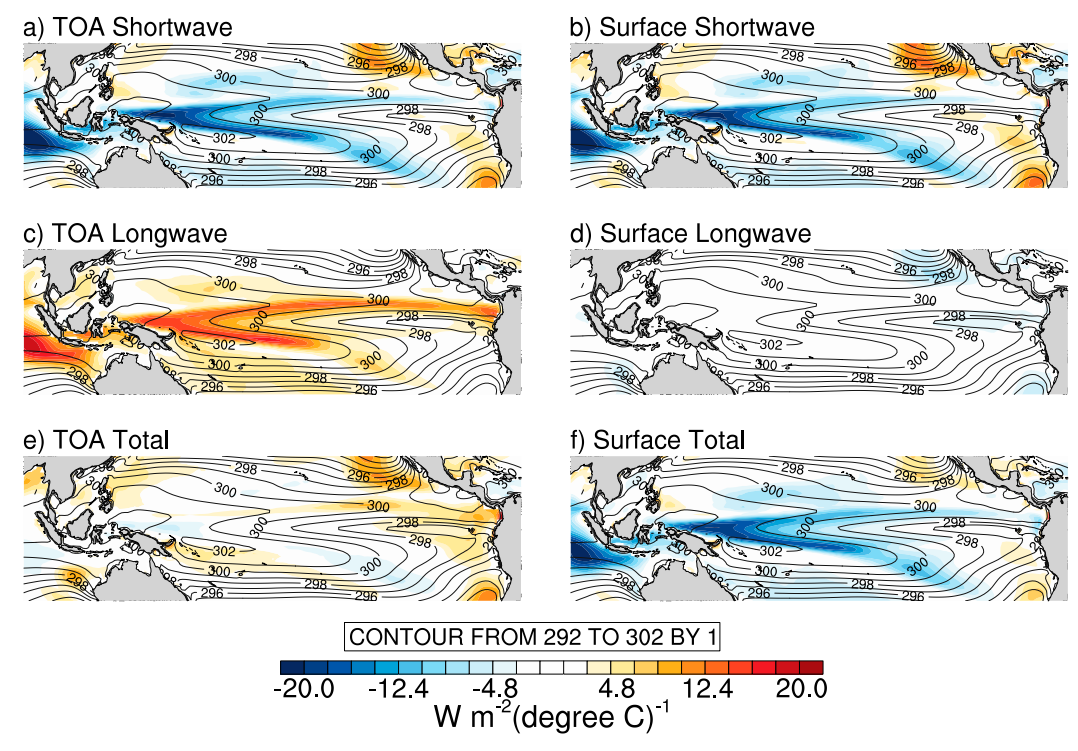


FIG. 2. (right) Surface and (left) top-of-atmosphere (TOA) components of cloud radiative feedback in CESM1.2. Cloud radiative feedback is calculated as the pointwise regression of cloud radiative forcing onto sea surface temperature (SST) anomalies (colors) and from the preindustrial control CESM1.2 simulation. Cloud radiative feedback components are divided into (top) shortwave, (middle) longwave, and (bottom) total (shortwave plus longwave) components. All radiative forcing values are defined as positive down. Climatological SST, calculated over the entire duration of the control simulation, is overlaid (contours).

used extensively (Lloyd et al. 2009, 2011, 2012; Chen et al. 2013; Bellenger et al. 2014; Kim et al. 2014; Li et al. 2015; Rädel et al. 2016; Ferrett et al. 2018), though it has drawbacks (Soden et al. 2004). The calculation of CRE as all-sky minus clear-sky radiative fluxes may contain the effects of cloud-masking, which may bias the true cloud radiative feedback (Soden et al. 2004). For example, water vapor or the temperature profile within a cloud may offset radiative balance differently than within clear skies (Zhang et al. 1994). For the purpose of this study, we are simply using it as a way to gauge the degree of CRFB on climate variability and are not considering feedbacks between CRE, water vapor, and temperature. For a fair comparison of CRFBs in other CMIP multimodel analyses (Lloyd et al. 2009, 2011, 2012; Chen et al. 2013; Bellenger et al. 2014; Kim et al. 2014; Li et al. 2015; Rädel et al. 2016; Ferrett et al. 2018), we maintain consistency and also use the regression of CRE on SST.

3. Results and discussion

We isolate the role of CRFB in ENSO events by comparing the control simulation, where CRFBs are active

(CRFB \neq 0), to the cloud-locked experiment, where CRFBs are disabled (CRFB = 0). The control simulation shows predominantly negative CRFB on SST (CRFB < 0) through the tropics and subtropics at the surface, which indicates that negative shortwave CRFB (SW CRFB) dominates the surface response in this model (Figs. 2b,d,f). Observations and CESM1.2 both show that SW CRFB dominates at the surface (Figs. 1 and Figs. 2), exceeding LW CRFB by $8.58 \,\mathrm{W \, m^{-2}}$ in the Niño-3.4 region (Fig. 2f). CESM1.2 produces a CRFB spatial pattern that is slightly different from observations and underestimates total SW CRFB $(-8.61 \,\mathrm{W\,m^{-2}})$ in observations vs $-5.52 \,\mathrm{W\,m^{-2}}$ in CESM1.2 in the Niño-3.4 region). With cloud-locking, CRFBs in Fig. 2 nearly vanish (Fig. S3). We will show that negative SW CRFB on SSTA dominates the response to cloud-locking in CESM1.2, which is a different result from cloud-locking in a different state-of-the-art climate model [i.e., the MPI-ESM-LR as used in Rädel et al. (2016)].

a. Impact of CRFBs on the spatial pattern of the peak of El Niño and La Niña events

The change in the spatial pattern of the surface and atmospheric response during the peak of El Niños and

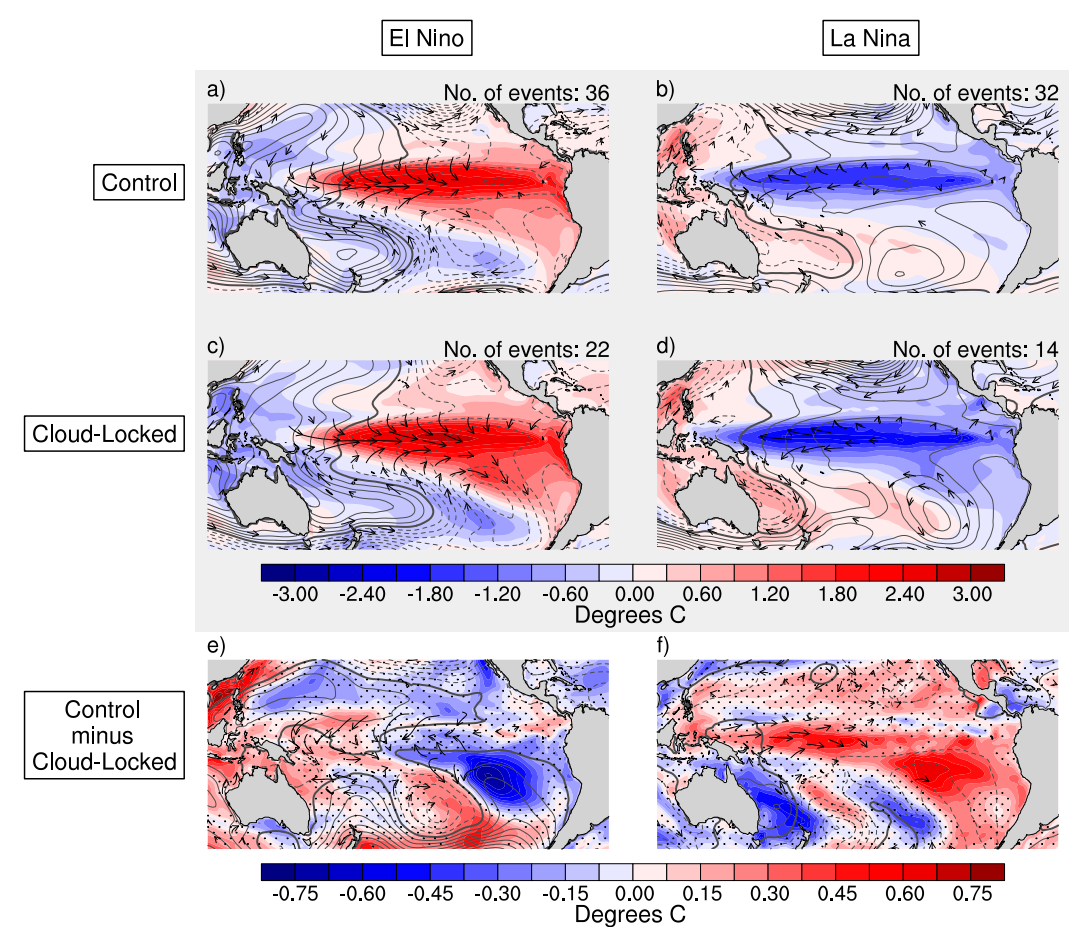
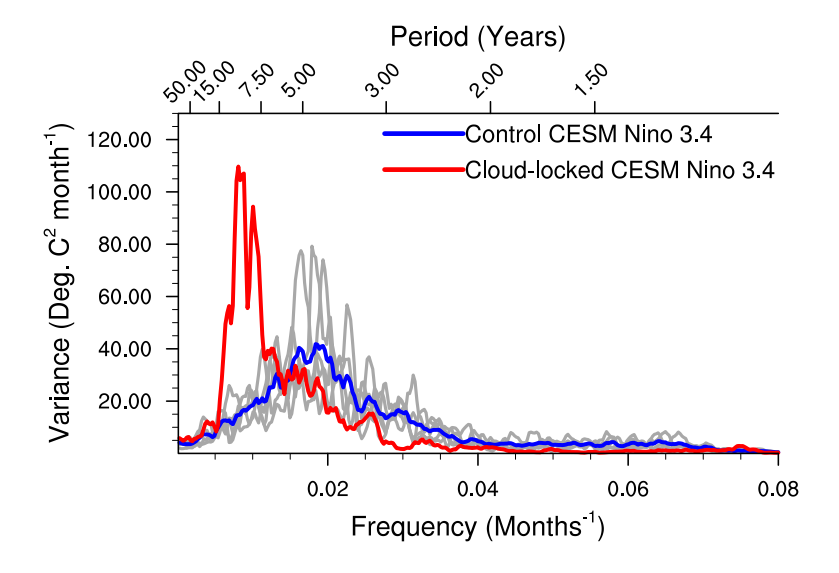


FIG. 3. Composites of SSTA, anomalous surface winds, and anomalous sea level pressure during the peak (DJF) of (left) El Niño and (right) La Niña events in (top) the control, (middle) cloud-locked, and (bottom) the control minus cloud-locked simulations. The selection of El Niño and La Niña events is described in section 2. Dots indicate where changes in SSTA due to cloud-locking are *not* statistically significant at the 95% level by a Student's t test (see the appendix for more details). Winds are only plotted if they exceed one standard deviation of the total wind speed from the corresponding experiment. Sea level pressure contours are plotted from -3 to 3 hPa in increments of 20 hPa.

La Niñas shown in Fig. 3 illustrates that negative SW CRFB is likely dominant at the peak. We isolate the SST anomalies impacted by interactive CRFBs (Figs. 3e,f) by subtracting the peak SSTA in the cloud-locked simulation (Figs. 3c,d) from the control simulation (Figs. 3a,b), so the differences should be interpreted as due to the inclusion of CRFBs. Overall, the SSTA caused by CRFBs are opposite sign of the ENSO-related SSTA. This suggests that CRFBs are damping ENSO-related SSTA; specifically, negative SW CRFB must be active during the peak of both El Niños and La Niñas. During El Niños, the southeast Pacific region is the most noticeable region where CRFBs significantly decrease the magnitude of peak SSTA (Figs. 3a,c,e). CRFBs significantly weaken the strength of La Niñas throughout most of the cold-tongue region, including the region west of the date line as well as the southeast Pacific region

(Figs. 3b,d,f). The fact that CRFBs impact western equatorial SSTA more during La Niñas than during El Niños reflects the impact of CRFBs associated with westward displacement of convection associated with the Walker circulation during La Niñas. We will revisit the potential role of the SE Pacific region in the next section. The fact that the SSTA spatial pattern due to CRFBs (Figs. 3e,f) are of opposite sign of SSTA during El Niños (Fig. 3a) and La Niñas (Fig. 3b) suggests that negative shortwave CRFB, rather than positive SW CRFB, is most important for the average SSTA across ENSO events. If positive SW CRFB was important for SSTA during the peak of El Niños or La Niñas, we would expect to see values that are of the same sign as the control simulation in the panels shown as Figs. 3e and 3f, which would indicate that SSTAs are enhanced when CRFBs are active.



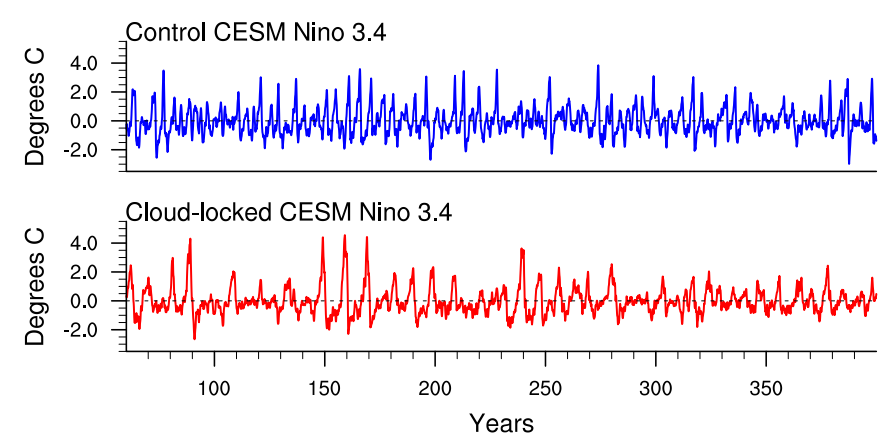


FIG. 4. (top) Power spectra and (bottom) time series of Niño-3.4 index from the control (gray and blue) and cloud-locked (red) simulation. Gray lines are the power spectra of five 350-yr swaths of the Niño-3.4 index from the control simulation. The blue line on power spectra is the average across swaths.

Additionally, the numbers of El Niño and La Niña events are displayed over each composite in Fig. 3. These are calculated over the entire cloud-locked simulation but only over one 370-yr period in the control simulation. The results are independent of which 370-yr period is chosen from the control simulation. Clearly, the cloud-locked simulation generates fewer El Niño and La Niña events than a time period of the same length in the control simulation. We will show that this is because both El Niño and La Niña events have longer duration in the simulation without CRFBs.

b. Change in periodicity of ENSO

CRFBs in CESM1.2 shorten the period of ENSO as indicated by the power spectra of the Niño-3.4 index in Fig. 4. The period of SSTA shifts from decadal time

scales when CRFBs are disabled to 3-7-yr time scales when CRFBs are active (Fig. 4). We interpret this merely as a shift in variance and a not change in total variance because the changes in total variance were not significant for any Niño indices (Table 2) at the 95% level by an F test. The result that CRFBs decrease ENSO periodicity is also evident in the power spectra of the Southern Oscillation index, an index of anomalous sea level pressure, in Fig. S4. Additionally, the relationship between Niño-3.4 and total ocean heat convergence in the Niño-3.4 region has the same phasing despite whether CRFBs are active; that is, ocean heat convergence leads Niño-3.4 SSTAs (see Fig. S5). However, we find that interactive CRFBs lead to a smaller convergence of heat in the ocean and smaller Niño-3.4 SSTAs as a result. Active CRFBs lead to approx.

TABLE 2. Statistics of various Niño indices from both control and cloud-locked simulation. The unit for variance is degrees Celsius squared, while skewness and kurtosis are unitless. Please see the appendix for a description of statistical significance and interpretation of skewness and kurtosis values.

	Variance	Skewness	Kurtosis
		Niño-4	
Control	0.731	0.129	-0.291
Cloud-locked	0.820	0.437	-0.037
		Niño-3.4	
Control	0.839	0.607	0.859
Cloud-locked	0.882	1.156	2.566
		Niño-3	
Control	0.725	0.593	1.019
Cloud-locked	0.760	1.163	3.159
		$Ni\tilde{n}o-1+2$	
Control	0.731	0.129	-0.291
Cloud-locked	0.820	0.437	-0.037

5 W m⁻² less ocean heat convergence at the peak and corresponding Niño-3.4 SSTAs are approx. 0.7°C cooler at the peak as well (top vs bottom panels in Fig. S5). Thus, there is evidence in both oceanic and atmospheric components that CRFBs lead to smaller and shorter ENSO events.

The change in periodicity due to disabling CRFBs is surprising because, typically, CRFBs are thought to act instantaneously on SSTA or on convection. Guilyardi et al. (2004) found a change in ENSO periodicity when coupling various CMIP3 atmospheric models to one ocean model, but these authors do not provide a conclusive statement on what specific mechanism controls the periodicity. We will provide evidence that CRFBs impact the periodicity by impacting the amount of incident SW radiation reaching the surface both on and off the equator.

c. CRFBs modulate the amount of incident solar radiation reaching the surface

The most direct way clouds may be impacting the duration of ENSO events is through their control on incident solar radiation reaching the surface, or the amount of heat reaching the ocean subsurface. The recharge–discharge oscillator theory poses that equatorial heat buildup during an El Niño event discharges by transitioning to La Niña, which is accomplished by anomalous heat transport by Sverdrup transport (Jin 1997). Convection occurs over the warmest SSTA, and clouds associated with this convection block incident radiation, providing a negative feedback on SSTA but also preventing heat from reaching the ocean subsurface. Without clouds forming in response to warm SSTA as in the cloud-locking configuration, incident solar radiation continues to reach the ocean surface and

subsurface, allowing more heat to build up. This additional heat buildup would lead to a longer decay time due to the fact that more heat transport is required to reach a neutral state. In other words, clouds prevent ocean subsurface heat buildup and thus a smaller, shorter El Niño event occurs.

Figure 5 illustrates this hypothesis with the composite of the progression of SSTA and anomalous SW cloud radiative forcing during El Niño events. We focus on El Niño events, but a similar mechanism occurs during La Niña events, which is pictured in Fig. S6. In the control simulation, dotted contours represent anomalous negative SW cloud forcing, or incident radiation reflected by anomalous convective clouds forming over warm SSTA (left panels, Fig. 5). As the El Niño event matures (from JJA⁰ to DJF¹), the maximum reflected SW radiation increases and remains over the maximum SSTA due to negative SW CRFB on SSTA (left panels, Fig. 5). In the cloudlocked simulation, convective clouds may not radiatively respond to warming SSTA, so they will not block incident solar radiation over the warmest SSTA (right panels, Fig. 5). Instead, climatological incident radiation continues to reach the surface (cf. left and right panels, MAM⁰ through MAM¹, Fig. 5), warming the ocean surface and subsurface. As the control simulation begins to transition to La Niña in the summer following the peak of the event (JJA¹, left panel, Fig. 5), the reflected SW cloud radiative forcing disperses, and by the winter of the following year (DJF², left panel, Fig. 5), incident radiation is reaching the surface over the anomalously cool equatorial SSTs associated with a La Niña event. During this period in the cloud-locked simulation, warm SSTA linger; there is no evidence of a transition to La Niña (right panels, JJA¹ through DJF²; Fig. 5). The SSTA noticeably weakens over the course of the following year, but the sign of the SSTA remains warm because more heat has to be removed from the system.

Changing the negative SW CRFB on SSTA is essentially one way to alter the damping rate of the system. Zebiak and Cane (1987) found that decreasing the surface flux feedback (analogous to removing the cloud SW damping) produces an "enormous" effect in their 1.5-layer shallow water model [also noted in Zebiak (1985)]. These authors observed a response similar to that described here for CESM1.2 (i.e., the periodicity and magnitude of the Niño-3 index increases), despite their use of a much simpler model. Neither Jin (1997) nor Zebiak and Cane (1987) explicitly characterize the atmospheric damping as negative SW CRFB, but our results show that this is an integral part of the net surface flux damping of SST.

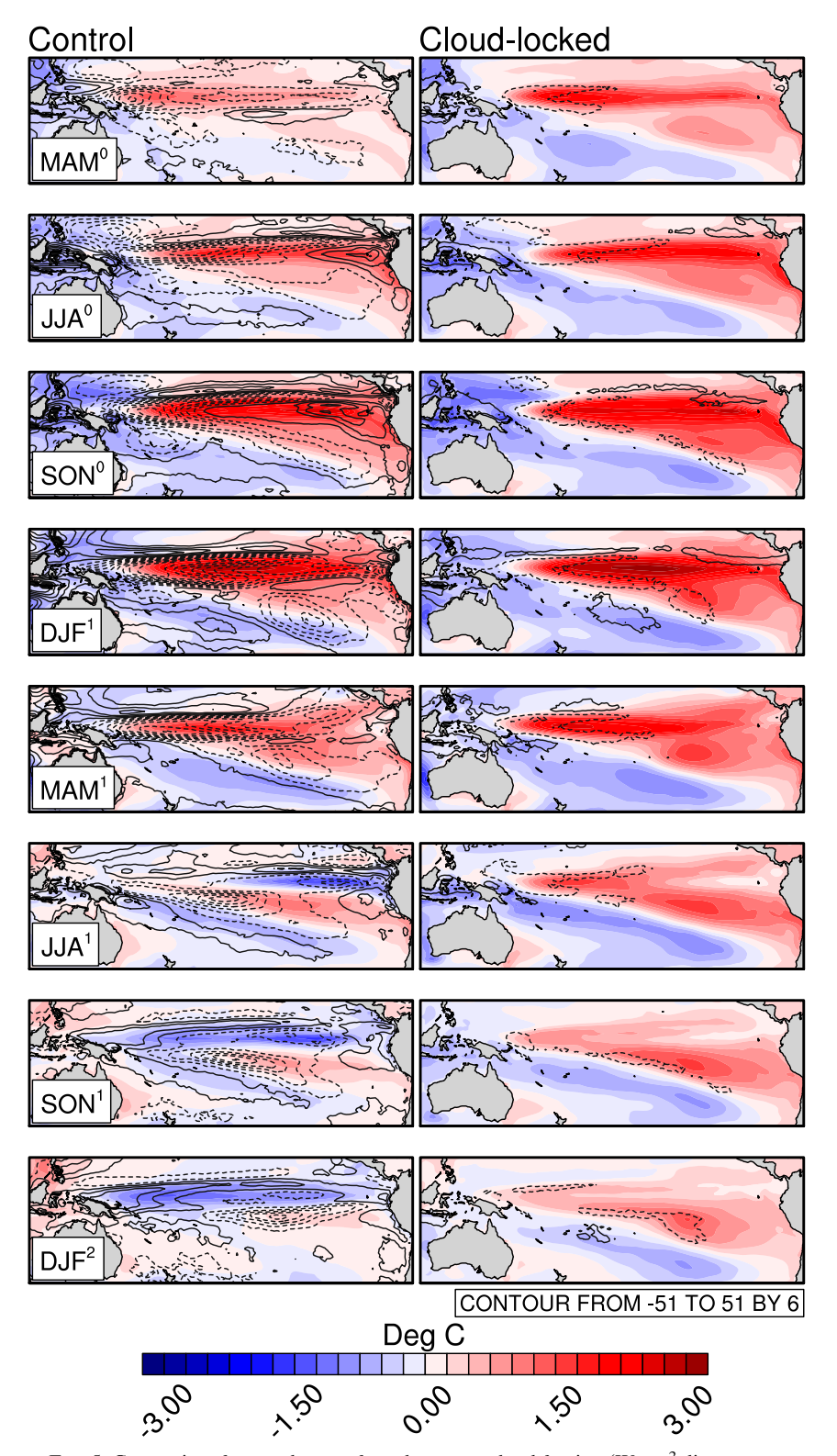


FIG. 5. Composite of anomalous surface shortwave cloud forcing (W m $^{-2}$; line contours; solid indicates positive down) overlaying anomalous sea surface temperature (°C; colored contours) during the seasons leading up to and following the peak of the El Niño event (DJF 1) in (left) the control simulation and (right) the cloud-locked simulation. All fields are standardized by the standard deviation of the Niño-3.4 index. Composite La Niña events are shown in Fig. S6.

d. CRFBs weaken off-equatorial westerly wind anomalies

CRFBs significantly dampen ENSO-related SSTA in the subtropical southeast (SE) Pacific (Figs. 3e,f), and a few previous studies suggest that this region may remotely influence the tropical Pacific climate variability or trigger El Niño events (Matei et al. 2008; Zhang et al. 2014; Larson et al. 2018). Partial coupling experiments utilizing coupled GCMs found that prescribing localized warming in the southern subtropical Pacific led to warmer SSTA in the equatorial Pacific on the order of \sim 1°C (Liu and Yang 2003; Matei et al. 2008). Matei et al. (2008) further noted that warming the subtropical SE Pacific led to a reduction in interannual standard deviation of SSTA by 30% and a shorter ENSO period. These authors attributed the change in ENSO period to the impact of thermal forcing from the SE Pacific on the strength of the equatorial Pacific annual cycle: a warmer SE Pacific strengthens the equatorial annual cycle and broadens the Niño-3 SSTA power spectra, and a cooler SE Pacific weakens the annual cycle, permitting lowfrequency Niño-3 SSTA variability (their Fig. 10). In our model, shorter-time scale variability in Niño-3.4 SSTA, apparent with interactive CRFBs, corresponds to SE Pacific SSTA that are cooler than the configuration with disabled CRFBs and a longer Niño-3.4 SSTA time scale (Figs. 3 and Figs. 4). This contradicts the results of Matei et al. (2008). On the other hand, the results of the two studies are not directly comparable because the changes in the southeastern Pacific SSTA due to cloud-locking in CESM1.2 (Figs. 3e,f) are time-varying, while the changes Matei et al. (2008) prescribed are a constant change to the mean state SST.

Other studies have considered not just the effect of the mean subtropical SE Pacific SST on ENSO-related SSTA variability but also specifically the role of variations in atmosphere-ocean coupling from the South Pacific meridional mode (SPMM) (Zhang et al. 2014; Larson et al. 2018). While we do not explicitly consider the SPMM in these simulations, an SPMM-like pattern appears in the cloud-locked simulation throughout the duration and following El Niño events (right panels, Figs. 5 and Figs. 6). The positive phase of the SPMM is characterized by a warm anomaly in the SE Pacific that propagates northwestward through the wind-evaporation-SST (WES) feedback. Zhang et al. (2014) showed that, in model configurations with atmospheric global climate models coupled to a slab ocean (AGCM-slab), the SPMM propagates westerly wind anomalies into the equatorial Pacific, producing ENSO-like SSTA variability. Recently, Larson et al. (2018) found that, by removing mechanical wind forcing in CCSM4, variability in the Niño-3.4 index

is thermally forced by positive latent heat flux from the SPMM. These authors further showed that the most positive Niño-3.4 anomalies lag with a positive-phase SPMM by a few months. While both of these mechanisms of the SPMM on ENSO posed by Zhang et al. (2014) and Larson et al. (2018) describe how SPMM may initiate ENSO events, our results suggest that an SPMM-like pattern found in our model may also help affect the persistence of ENSO anomalies. CRFB damp SSTA in the SE Pacific, removing a potential source of SSTA persistence from the region where SPMM originates. Without CRFBs, the warm SSTA in the SE Pacific lingers, which may lead to increased SPMM events, enhanced westerly winds at the equator, and a prolonged El Niño as a result (MAM¹ through SON¹ in Fig. 6).

Alternatively, CRFBs may influence westerly winds along the SPMM by influencing the southwestnortheast (SW-NE) SSTA gradient. The SW-NE SST gradient in the SE Pacific is weaker when cloud radiative feedbacks are active (cf. left and right panels in Figs. 5 and Figs. 6), which would otherwise sustain westerly wind anomalies. In the right panels of Fig. 6, the SSTA gradient along the SPCZ strengthens, which sustains westerly wind anomalies (MAM¹ through SON¹ in the right panels of Fig. 6) along the SW-NE SSTA gradient and causes warm SSTA to persist. These westerly wind anomalies are nearly absent when cloud radiative feedbacks are active (Fig. 5). The mechanism through which cloud radiative feedbacks weaken the SW-NE SSTA gradient in the southeast Pacific remains unclear, but such a gradient associated with SPMM-like winds acts to reduce a remote source of persistence of ENSOrelated equatorial SST anomalies.

e. CRFBs influence ENSO periodicity through offequatorial wind stress anomalies

Despite the uncertainty of the mechanism through which CRFBs impact off-equatorial westerly wind anomalies, enhancing these winds lengthens ENSO periodicity. Kirtman (1997) showed that widening the meridional scale of westerlies in an idealized GCM lengthens ENSO period by initiating lower-frequency Rossby waves. We show directly that CRFBs weaken off-equatorial wind stress important for the lengthening the periodicity of ENSO. Figure 7 shows the anomalous zonal wind stress regressed on the Niño-3.4 index from the control simulation with CRFBs (Fig. 7a) and then the difference between the cloud-locked pattern from the control pattern to isolate the role of CRFBs (Fig. 7b). Figure 7b shows that CRFBs cause stronger off-equatorial easterly wind stress anomalies (purple contours and negative values on black zonal mean line plot), that is, a reduction in the off-equatorial westerly

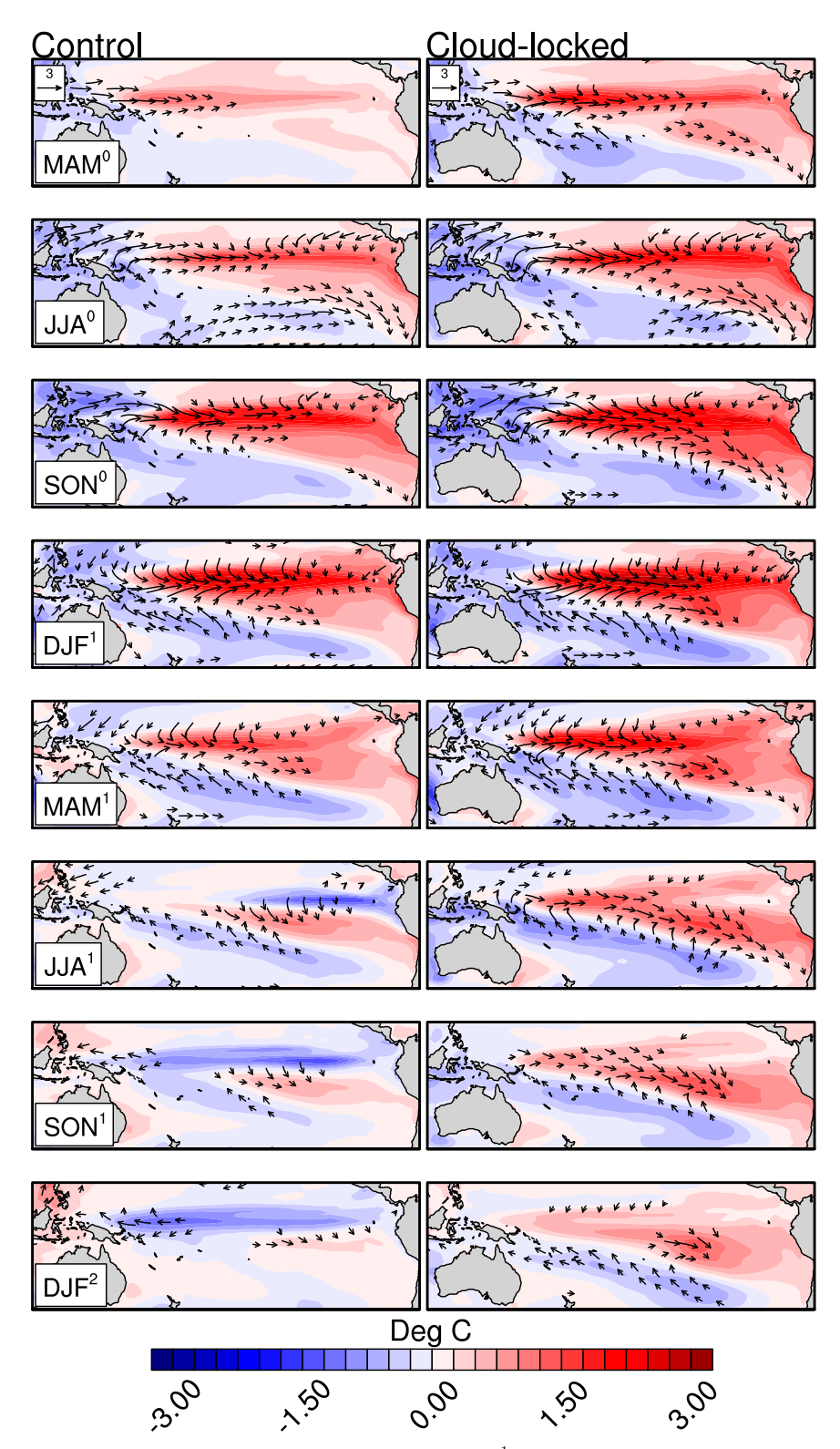


FIG. 6. Composite of anomalous surface wind (m s $^{-1}$; vectors) overlaying anomalous sea surface temperature (°C; colored contours) during the seasons leading up to and following the peak of the El Niño event (DJF 1) in (left) the control simulation and (right) the cloud-locked simulation. Only winds that exceed 1 m s $^{-1}$ are plotted. Composites of corresponding SSTA and anomalous surface winds during La Niña events are shown in Fig. S7.

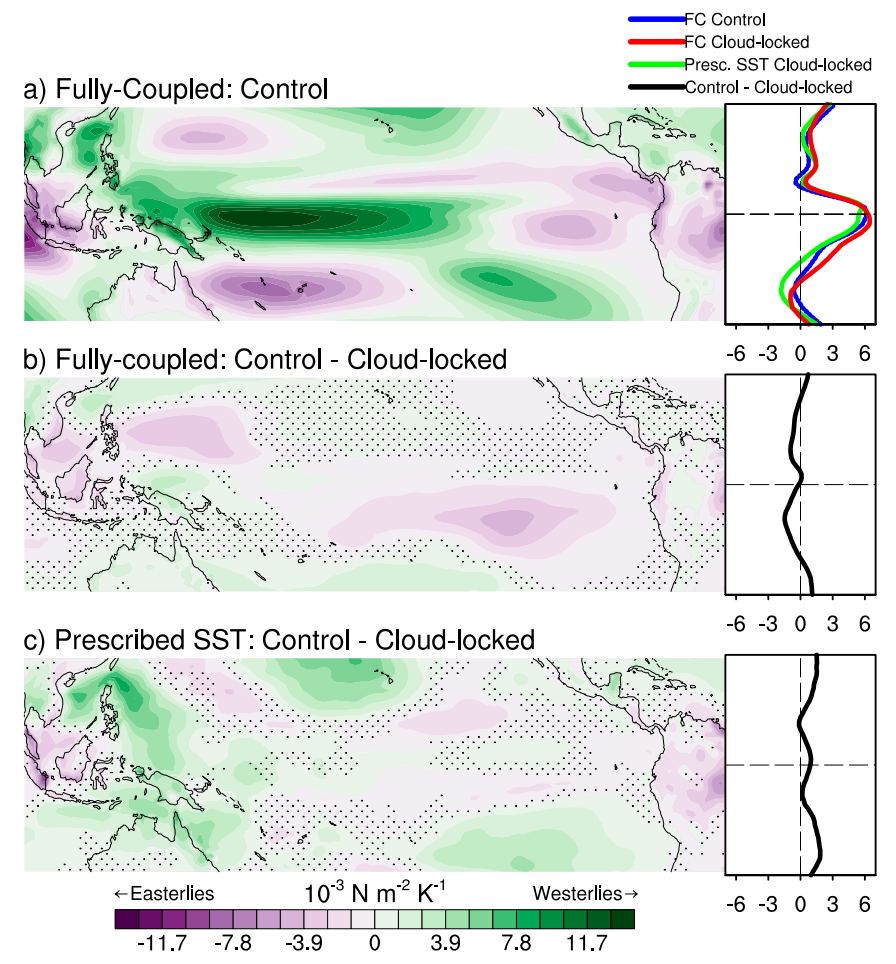


FIG. 7. The regression of the anomalous zonal wind stress onto the Niño-3.4 index in (top) the fully coupled control simulation and (middle) the difference in regression patterns, calculated as the control minus cloud-locked simulation, in the fully coupled simulation and (bottom) the prescribed SST simulation. The zonal means of both simulations' regression patterns are indicated to the right of the top panel, and the difference (control minus cloud-locked) between the zonal mean regression panels is shown to the right of the bottom panel. Green values indicate westerly wind stress and purple indicates easterly. Stippling indicates where the differences in correlation of zonal wind stress and Niño-3.4 index between the two experiments are *not* significant by a z score obtained through Fisher-Z transformation at the 95% significance level. Details on statistical significance testing are discussed in the appendix.

wind stress that would force Rossby waves (Kirtman 1997). Thus, in the simulation with CRFBs, the meridional width of westerly stress is narrower, and the period of ENSO is shorter.

The impact of the changes in off-equatorial wind stress by CRFBs is further demonstrated by prescribing the wind stress from either simulation in an idealized model. This model is composed of Zebiak and Cane (1987) ocean model (i.e., a linear reduced gravity ocean model forced by a simple statistical atmosphere). The atmospheric forcing contains a net surface heat flux damping term, which restores the SSTA to zero, as well as a linear forcing from the pattern of surface wind stress

regressed on local SSTA. A more detailed description of this idealized model can be found in Kirtman and Schopf (1998) and Kirtman (1997). First, we prescribe the pattern of wind stress from the entire Pacific basin regressed on the Niño-3.4 index from the control simulation and the cloud-locked simulations separately in the model. The differences in Niño-3.4 index variability between these two experiments isolate the impact of changes in ENSO-related wind stress due to disabling CRFBs. Figure 8 shows that the wind stress occurring in the model with CRFBs active leads to a Niño-3.4 period that is nearly half (blue solid line) that of the wind stress pattern in the model configuration without CRFBs (red

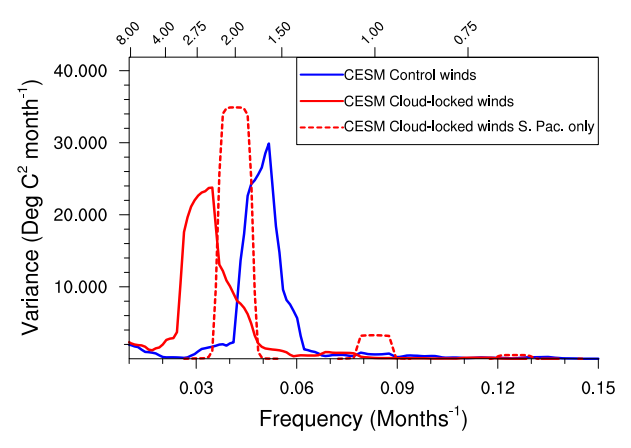


FIG. 8. Power spectra of Niño-3.4 index from idealized model simulations with prescribed wind stress patterns taken from control (blue) and cloud-locked (red) CESM1.2 simulations. The top *x* axis indicates the period in years. The blue line indicates the Niño-3.4 power spectrum from the simulation prescribed wind stress forcing with cloud feedbacks active, and the red lines indicate the results from prescribing wind stress from the cloud-locked simulations. The dotted red line indicates the result of prescribing the wind stress pattern only in the subtropical southeast Pacific. For more details on the idealized model configuration and the calculation of the wind stress patterns, please see section 3e.

solid line). Based on Figs. 3, 6, and 7, we suspect that the winds in the southeast Pacific region may impact the periodicity of the Niño-3.4 index. To isolate their role, we prescribe the wind stress pattern from the cloud-locked experiment only in the southeast Pacific region (within 20°S to the equator and 175°–80°W). The region boundaries are based on the location of maximum SSTA change due to cloud-locking. We find that the wind stress pattern in this region explains around approximately two-thirds of the shift in periodicity without CRFBs (dotted red line vs solid red line, Fig. 8), suggesting that wind stress changes in the SE Pacific alone can cause a significant change in ENSO periodicity.

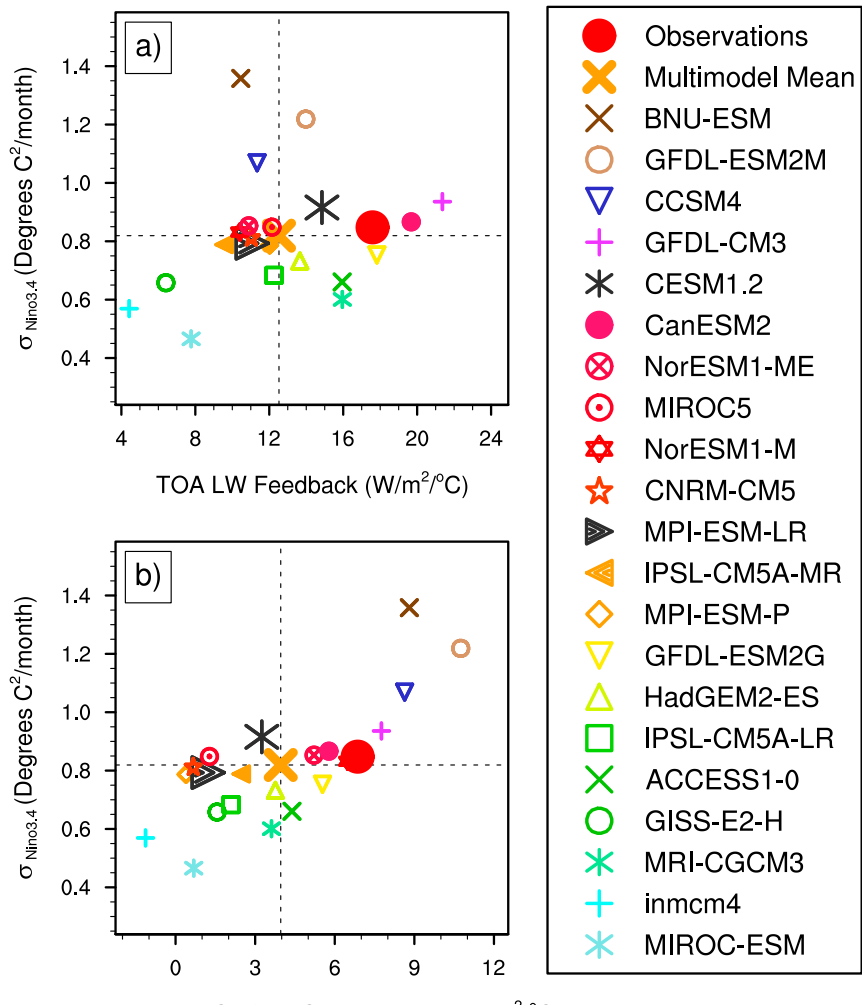
f. The role of CRFBs in ENSO in other models: LW CRFB on circulation

Traditionally, a multimodel analysis is used to compare and search for dominant feedbacks that contribute to ENSO variability but can be misleading due to the correlation among numerous feedbacks on ENSO SSTA. For example, one study considers positive LW CRFB on circulation important for ENSO SSTA variability (Rädel et al. 2016). Figure 9a shows the correlation between the magnitude of positive LW CRFB on SSTA and Niño-3.4 SSTA variance (R = 0.223). One may conclude from this positive correlation that the magnitude of positive LW CRFB on SSTA is a good predictor of Niño-3.4 variance (i.e., the larger the

positive LW CRFB, the larger the SSTA variance). If this is the case, SSTA variability should decrease if that models' LW CRFB is zero. Indeed, this response is observed in the MPI-ESM-LR model when cloud-locking is implemented (Rädel et al. 2016). These authors posit that the positive LW CRFB on circulation enhances the anomalous Walker circulation during an El Niño event, thus enhancing the Bjerknes feedback and SSTA variance as a result. These authors find that, when CRFBs are removed through cloud-locking, SSTA variance decreases across all time scales. According to Fig. 9a, CESM1.2 (marked with a large black asterisk) has a larger positive LW CRFB (14.85 W m⁻² °C⁻¹) than that of the MPI-ESM-LR model (large black right-pointing triangle; $11.08 \,\mathrm{W\,m^{-2}\,^{\circ}C^{-1}}$), so a valid hypothesis is that the response of cloud-locking in CESM1.2 will also be a decrease in tropical SSTA variance across all time scales. But alas, cloud-locking in CESM1.2 results in an insignificant change in total variance, producing instead a shift of variance from short to long time scales (Table 2; Fig. 4).

CESM1.2 still produces a LW CRFB on circulation as the MPI-ESM-LR model, but either the feedback dominates Niño-3.4 variance on interannual time scales or its influence on the total surface response to ENSO is dominated by other SSTA feedbacks. The LW CRFB on circulation in CESM1.2 is evident when we reproduce Fig. 3a from Rädel et al. (2016) in our Fig. 10. The CESM1.2 control simulation shows that the anomalous Walker circulation strengthens (dashed contours, Fig. 10c) and atmosphere anomalies aloft warm more in response to Niño-3.4 anomalies than that of the cloudlocked simulation (red filled contours, Fig. 10c). This is consistent with the result of cloud-locking in the MPI-ESM-LR model as well (Rädel et al. 2016), namely that the positive LW CRFB on atmospheric circulation enhances the anomalous Walker circulation and anomalously warm atmospheric temperature related to ENSO. There is evidence that positive LW CRFB could be influencing the surface response of ENSO in CESM1.2: SSTA variance is enhanced by CRFBs but only on 2-6yr time scales (Fig. 4). Therefore, the impact of certain CRFBs may depend on the period.

Additionally, the balance of ENSO feedbacks may determine which CRFBs exert influence over the surface ENSO response, and this balance may differ among models. To show that LW CRFB on the circulation's influence over surface ENSO variability competes with SSTA feedbacks, we reproduce cloud-locking in a simulation with prescribed SSTs and observe the response in ENSO-related zonal wind stress (Fig. 7c). We use full-field, time-varying SSTs from the control fully coupled simulation for both control and cloud-locked simulations.



Asymmetry in Surface SW Feedback (W/m²/°C)

FIG. 9. Intermodel comparison of the magnitude of Niño-3.4 index, represented by the standard deviation (y axis), against cloud radiative feedback metrics (x axis). (a) The Niño-3.4 magnitude against longwave cloud radiative feedback, calculated with top-of-atmosphere longwave cloud radiative forcing regressed on the Niño-3.4 index, averaged across the Niño-3.4 region. (b) The Niño-3.4 magnitude against asymmetry in shortwave cloud radiative feedback, calculated as the difference between the regression of surface shortwave cloud radiative forcing on positive and negative Niño-3.4 anomalies, averaged across the Niño-3.4 region. Feedbacks in CESM1.2 and MPI-ESM-LR are represented by a large black asterisk and right-pointing-triangle, respectively. Observations are indicated by the large red dot. Multimodel mean is indicated by large orange "X". The R^2 value for (a) is $R^2 = 0.050$ and is insignificant at the 95% level by t test; for (b), t00 and is significant. Additional details on significance tests can be found in the appendix.

Both the control and cloud-locked simulations with prescribed SSTs are 97 years long. We also prescribe the same cloud field in the cloud-locked simulation as was used in the fully coupled cloud-locked simulation. In both prescribed SST configurations, SSTAs are evolving identically to the fully coupled control simulation, but unlike the fully coupled configuration, there are no atmospheric feedbacks on SSTA—including

SW CRFB on SSTA or the Bjerknes feedback because there is no atmosphere–ocean (AO) coupling. Any changes in ENSO surface winds due to cloud-locking must be caused by disabling CRFB on circulation (e.g., the LW CRFB on circulation) rather than CRFBs on SSTA (e.g., the SW CRFB on SSTA). By comparing the cloud-locked prescribed SST simulation to the clouds-active prescribed SST simulation, we find a

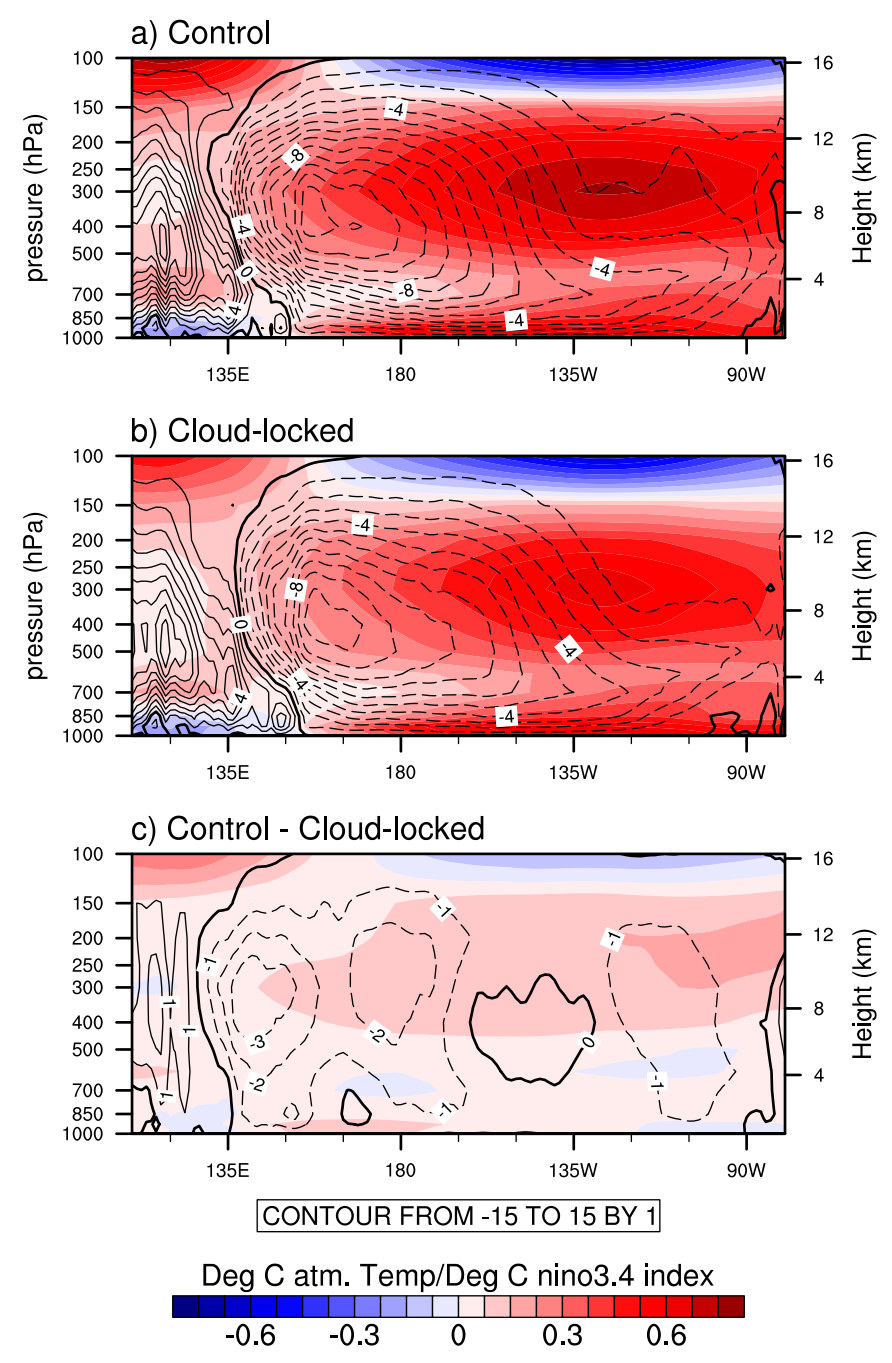


FIG. 10. Anomalous atmospheric temperature (colored contours) and vertical velocity (hPa day⁻¹ °C; line contours; dashed indicates anomalous convection) averaged between 5°S and 5°N regressed onto the Niño-3.4 index from the (a) control and (b) cloud-locked simulations. (c) Contributions due to cloud radiative feedbacks are indicated by subtracting the cloud-locked simulation, where cloud radiative feedbacks are inactive, from the control simulation, where cloud radiative feedbacks are active.

result consistent with that of Rädel et al. (2016): the response of westerly wind stress to Niño-3.4 variability is enhanced by CRFBs at the equator (green filled contours, Fig. 7c). Furthermore, the response is enhanced

by CRFBs off the equator as well (green filled contours and positive values on zonal mean plot in Fig. 7c), which means CRFB on circulation could potentially be enhancing low-frequency ENSO periodicity and counteracting

the mechanisms posed in previous sections. In summary, CRFBs influence ENSO-related surface wind stress variability in a prescribed SST simulation (Fig. 7c) opposite to that in a fully coupled simulation (Fig. 7b; also see green and red lines on zonal mean line plot on Fig. 7a), which means SSTA ENSO feedbacks are competing with CRFBs for surface ENSO variability. In the case of the MPI-ESM-LR model, the balance between CRFBs and other ENSO feedbacks is probably different than that presented here for CESM1.2, resulting in a different role for CRFBs on ENSO variability at the surface of the equatorial Pacific.

g. The role of CRFBs in ENSO in other models: The asymmetry of SW CRFB on SSTA

Another cloud-related predictor of Niño-3.4 variance in CMIP5 models presented in the literature is SW CRFB asymmetry (Fig. 9b) (Lloyd et al. 2009, 2012; Bellenger et al. 2014), which may provide better insight on the role of CRFBs and ENSO SSTA variance. SW CRFB asymmetry is due to the fact that negative SW CRFB on positive SSTA is larger in magnitude than positive SW CRFB on negative SSTA and is important because SW CRFB on SSTA changes sign during the course of ENSO (Lloyd et al. 2012). The SW CRFB changes from a negative during an El Niño to a positive during a La Niña event because of the zonal displacement in the Walker circulation, causing the convective regime over the Niño-3.4 region to shift from deep convection to subsidence (Lloyd et al. 2012; Bellenger et al. 2014). The SW CRFB asymmetry, calculated as the magnitude of the positive SW CRFB minus the negative SW CRFB, is highly correlated with ENSO magnitude across CMIP5 models, with R = 0.764 (Fig. 9b; Bellenger et al. 2014). In fact, the R^2 value of 0.584 is statistically significant at the 95% level using a t test (more details are provided in the appendix). Most CMIP5 models do a poor job of recreating the asymmetry from observations (large red dot in Fig. 9b), usually underestimating negative SW CRFB or even simulating a net positive SW CRFB (Lloyd et al. 2012; Chen et al. 2013; Kim et al. 2014; Bellenger et al. 2014; Li et al. 2015; Ferrett et al. 2018). The inability of models to capture this asymmetry is attributed to models' inability to shift between convective regimes during ENSO (Bellenger et al. 2014) as well as varying liquid water path and cloud cover to changing SSTs (Li et al. 2015; Tang et al. 2016; Ferrett et al. 2018). Studies have shown that asymmetry in the magnitude and duration of La Niña or El Niño may be due to the nonlinearity in the response of convection, and thus, SW CRFB, to SSTA (Hoerling et al. 1997; Okumura and Deser 2010). Cloudlocking in either MPI-ESM-LR or CESM1.2 does not

reveal a role for positive SW CRFB on SSTA for ENSO SSTA variability, so we cannot clarify the relationship between SW CRFB asymmetry and ENSO SSTA. But, considering the correlation between SW CRFB asymmetry and ENSO SSTA variability (Fig. 9b), and SW CRFB asymmetry's dependence on both convection and SSTA, perhaps this metric could guide our understanding on the relationship between CRFBs and ENSO SSTA.

In general, the discrepancies between cloud-locking in CESM1.2 and MPI-ESM-LR highlight the importance of understanding the role of cloud-convective feedbacks on ENSO (Bellenger et al. 2014). Convection has been connected to ENSO amplitude and periodicity (Guilyardi et al. 2004; Neale et al. 2008) and depends on other climate model biases as well (Chen et al. 2013; Kim et al. 2014).

4. Conclusions

We find that negative SW CRFB in the CESM1.2 plays an essential role in determining the frequency of ENSO events. By prescribing clouds in the radiation module of CAM5 in fully coupled CESM1.2, we successfully disable CRFBs to find that the periodicity of Niño-3.4 anomalies shifts from \sim 10-yr time scales when CRFBs are disabled to 2–7-yr time scales when CRFBs are active, resulting in smaller but more frequent ENSO events. We pose a few hypotheses for this response. At the peak of El Niño, negative SW CRFB over the largest SST anomaly maintains the magnitude and the length of the event by modulating heat flux into the upper ocean and preventing upper ocean heat buildup. Consistent with the recharge-discharge oscillator hypothesis, the system requires a longer period to discharge more heat without negative SW CRFB. Another two hypotheses involve off-equatorial winds. One is that a positive SPMM-like mode persists throughout the duration of the El Niño event without CRFBs (i.e., the positive SPMMlike mode is damped by CRFBs). Based on two previous studies linking the positive phase of the SPMM to initiate stronger Niño-3.4 variability, we hypothesize that negative SW CRFB dampens equatorial El Niño SSTAs by damping the positive phase SPMM. Last, CRFB in CESM1.2 weakens the off-equatorial westerly wind stress, which shortens the period of ENSO by inhibiting Rossby waves with longer period (Kirtman 1997).

Cloud-locking in CESM1.2 yields completely different results in ENSO magnitude due to cloud-locking than that of another cloud-locking study (Rädel et al. 2016). We find that, although positive LW CRFB on circulation is active in CESM1.2, it does not have a dominant influence on Niño-3.4 variability, whereas the other study concluded that LW CRFB was a crucial

ENSO cloud feedback for Niño-3.4 variance (Rädel et al. 2016). In CESM1.2, LW CRFB on circulation enhances the zonal wind stress response to ENSO SSTA, but this is only evident in a model without AO coupling, suggesting that other feedbacks are more important for the surface variability of ENSO.

From a multimodel analysis, one might conclude that both SW CRFB asymmetry and LW CRFB are good predictors of the magnitude of ENSO SSTA. However, our results show that the relationship between the magnitude of ENSO SSTAs and CRFBs cannot be determined without directly altering the CRFBs. One reason is because SW CRFB and LW CRFB are not independent from each other (and other feedbacks) and partially cancel each other out, so it is unclear which feedback dominates.

Even though cloud-locking may provide an idea of the sensitivity of ENSO to CRFB, cloud-locking may not necessarily shed light as to how to improve the simulation of CRFB because it disables CRFBs as a whole, and the implementation varies from model to model. For example, multimodel analysis points to intermodel spread in the response of convection (Lloyd et al. 2012; Ferrett et al. 2018), liquid water path (Li et al. 2015; Ferrett et al. 2018), or cloud cover (Lloyd et al. 2012; Li et al. 2015; Ferrett et al. 2018) as the source of intermodel spread in SW CRFB. Additional locking experiments are required to pinpoint what component of SW CRFB causes the most sensitivity in ENSO dynamics. Furthermore, the components of SW CRFB calculation vary from model to model, which means cloud-locking should be a tool developed in other models for intermodel comparison. Overall, the results of this study highlight how much there is yet to be learned about the relationship between CRFBs and ENSO dynamics.

Acknowledgments. This research was supported by the National Science Foundation Graduate Research Fellowship Program (NSF GRFP). This work would not be possible without the computational support and resources provided by the Computational Information Systems Laboratory (CISL) at National Center for Atmospheric Research (NCAR), as well as the various international modeling groups participating in CMIP5. NCAR is sponsored by the National Science Foundation. We express immense gratitude to Jerry Olsen for substantial help with implementing cloud-locking in CESM—this project would not exist without his efforts. We extend thanks to Thorsten Mauritsen for inspiring this experiment, answering many questions about cloud-locking, and openly sharing other cloud-locking experiments. We also thank the Climate Analysis Section at NCAR for extensive feedback that led to clearer plots. EM and AC were supported by National Oceanic and Atmospheric Administration (NOAA) Grant NA14OAR4310275. BM acknowledges support from the Regional and Global Climate Modeling Program of the U.S. Department of Energy, Office of Science, Cooperative Agreement DE-FC02-97ER62402. BK was supported by NSF Grant OCE1419561 and NOAA Grant NA15OAR4320064.

APPENDIX

Description of Statistical Significance Testing

a. Statistical significance in Fig. 3

We applied a Student's t test in testing the significance in the difference of composites of SSTA between the control and cloud-locked simulations (Fig. 3) during El Niño and La Niña events separately. The composites were of the DJF values during the peak of either event. The null hypothesis is that the composite DJF maps from the two simulations are from the same distribution of SSTA values during peak El Niño/La Niña events. The mean was simply the plotted composite SSTA, and the standard deviation was taken separately across DJF SSTA El Niño and La Niña events. Since these events are discrete and one event (take an El Niño event, for example) does not necessarily predict the next El Niño event, the degrees of freedom were taken as the number of El Niño events in each simulation (pictured in the top right-hand corner of panels Figs. 3a-d).

b. Table 2: Niño index statistics

(i) We used an F test to test whether the variances for each Niño index were significantly different between the control and cloud-locked simulations. We adjusted the sample size N to an effective N^* to account for autocorrelation within each respective Niño index (Leith 1973):

$$N^* = \frac{N}{2\tau},$$

where N is the length of the cloud-locked Niño index and τ is the e-folding time scale of the Niño index analyzed. Because the cloud-locked simulation is four times shorter in length (370 vs 1800 years), we computed the F test four times for each Niño index after splitting the control simulation into four 370-yr periods. The F test never yielded statistically significant probabilities (<5%) for more than two of the four tests conducted, so we cannot conclude that any of the variances between the control and cloud-locked Niño indices are significantly different.

(ii) In Table 2, both skewness and kurtosis for each Niño index from both simulations are listed. The skewness describes the symmetry of the distribution, where a value of 0.0 indicates the distribution is perfectly symmetrical, and a value greater than 0.0 indicates the positive values of the distribution are more likely. Kurtosis describes the flatness of the distribution, or the likelihood of extreme values of Niño-3.4 compared to small values. A normal distribution has a value of 0.0. A kurtosis value greater than 0.0 indicates that the distribution is wide and flat, and that the extreme values of Niño-3.4 are more likely than that of a normal distribution. Negative kurtosis values indicate that extreme values are less likely than that of a normal distribution.

c. Statistical significance in Fig. 7

We used a Fisher Z-transformation to test the significance of difference in the regression of zonal wind stress anomalies on the Niño-3.4 index between the control and cloud-locked simulations (Figs. 7b,c). The Fisher-Z transformation tests whether the difference between two correlations is nonzero. This is applicable to the difference in regressions because regression is just correlation multiplied by a scalar. This transformation makes no assumption about the distribution of the underlying data because it relies on the computation of a z score and uses the fact that Z is normally distributed. First, transformations for a correlation value from each simulation are computed using the following:

$$Z_{\text{CTRL}} = \frac{1}{2} \ln \left(\frac{1 + r_{\text{CTRL}}}{1 - r_{\text{CTRL}}} \right); \ Z_{\text{CLDLCK}} = \frac{1}{2} \ln \left(\frac{1 + r_{\text{CLDLCK}}}{1 - r_{\text{CLDLCK}}} \right).$$

Then, a z score is computed from the difference of means:

$$z = \frac{Z_{\text{CTRL}} - Z_{\text{CLDLCK}} - \Delta_{\text{CTRL,CLDLCK}}}{\sigma_{\text{CTRL,CLDLCK}}}.$$

Since our null hypothesis is that the two correlations are not significantly different, we assume the differences in the mean of the data ($\Delta_{\text{CTRL},\text{CLDLCK}} = \mu_{\text{CTRL}} - \mu_{\text{CLDLCK}}$) is zero. The term $\sigma_{\text{CTRL},\text{CLDLCK}}$ is calculated as

$$\sigma_{\rm CTRL,CLDLCK} = \sqrt{\frac{1}{N_{\rm CTRL}^* - 3} + \frac{1}{N_{\rm CLDLCK}^* - 3}},$$

where the effective degrees of freedom N^* are calculated over the Niño-3.4 index in each experiment as described in section b (item i) above.

d. Significance of linear relationship in Fig. 9

The significance of a linear relationship between cloud radiative feedbacks and Niño-3.4 indices across CMIP5 models in Fig. 9 is tested by computing a *t* statistic using

the correlation value computed for both Figs. 9a and 9b. The number of samples was the number of CMIP5 models included in the analysis (21). If the t statistic returned a probability smaller than 5%, we concluded that the correlation calculated is significant at the 95% level.

REFERENCES

- Battisti, D. S., and A. C. Hirst, 1989: Interannual variability in a tropical atmosphere–ocean model: Influence of the basic state, ocean geometry and nonlinearity. *J. Atmos. Sci.*, **46**, 1687–1712, https://doi.org/10.1175/1520-0469(1989)046<1687: IVIATA>2.0.CO;2.
- Bellenger, H., E. Guilyardi, J. Leloup, M. Lengaigne, and J. Vialard, 2014: ENSO representation in climate models: From CMIP3 to CMIP5. *Climate Dyn.*, **42**, 1999–2018, https://doi.org/10.1007/s00382-013-1783-z.
- Bellomo, K., A. Clement, T. Mauritsen, G. R\u00e4del, and B. Stevens, 2014: Simulating the role of subtropical stratocumulus clouds in driving Pacific climate variability. *J. Climate*, 27, 5119–5131, https://doi.org/10.1175/JCLI-D-13-00548.1.
- Bretherton, C. S., and A. H. Sobel, 2002: A simple model of a convectively coupled Walker circulation using the weak temperature gradient approximation. J. Climate, 15, 2907–2920, https://doi.org/10.1175/1520-0442(2002)015<2907:ASMOAC> 2.0.CO;2.
- Burgman, R. J., B. P. Kirtman, A. C. Clement, and H. Vazquez, 2017: Model evidence for low-level cloud feedback driving persistent changes in atmospheric circulation and regional hydroclimate. *Geophys. Res. Lett.*, 44, 428–437, https://doi.org/ 10.1002/2016GL071978.
- Ceppi, P., and T. G. Shepherd, 2017: Contributions of climate feedbacks to changes in atmospheric circulation. *J. Climate*, 30, 9097–9118, https://doi.org/10.1175/JCLI-D-17-0189.1.
- Chen, L., Y. Yu, and D.-Z. Sun, 2013: Cloud and water vapor feedbacks to the El Niño warming: Are they still biased in CMIP5 models? *J. Climate*, 26, 4947–4961, https://doi.org/ 10.1175/JCLI-D-12-00575.1.
- Clement, A. C., R. Burgman, and J. R. Norris, 2009: Observational and model evidence for positive low-level cloud feedback. *Science*, 325, 460–464, https://doi.org/10.1126/science.1171255.
- Dommenget, D., 2010: The slab ocean El Niño. *Geophys. Res. Lett.*, **37**, L20701, https://doi.org/10.1029/2010GL044888.
- Ferrett, S., M. Collins, and H.-L. Ren, 2018: Diagnosing relationships between mean state biases and El Niño shortwave feedback in CMIP5 models. *J. Climate*, **31**, 1315–1335, https://doi.org/10.1175/JCLI-D-17-0331.1.
- Guilyardi, E., and Coauthors, 2004: Representing El Niño in coupled ocean–atmosphere GCMs: The dominant role of the atmospheric component. *J. Climate*, 17, 4623–4629, https://doi.org/10.1175/JCLI-3260.1.
- Hoerling, M. P., A. Kumar, and M. Zhong, 1997: El Niño, La Niña, and the nonlinearity of their teleconnections. *J. Climate*, **10**, 1769–1786, https://doi.org/10.1175/1520-0442(1997)010<1769: ENOLNA>2.0.CO;2.
- Huang, B., and Coauthors, 2017: Extended reconstructed sea surface temperature, version 5 (ERSSTv5): Upgrades, validations, and intercomparisons. *J. Climate*, 30, 8179–8205, https://doi.org/10.1175/JCLI-D-16-0836.1.
- Hurrell, J.W., and Coauthors, 2013: The Community Earth System Model: A framework for collaborative research. *Bull. Amer.*

- *Meteor. Soc.*, **94**, 1339–1360, https://doi.org/10.1175/BAMS-D-12-00121.1.
- Jin, F.-F., 1997: An equatorial ocean recharge paradigm for ENSO. Part I: Conceptual model. J. Atmos. Sci., 54, 811–829, https://doi.org/10.1175/1520-0469(1997)054<0811:AEORPF>2.0.CO;2.
- Kay, J. E., and Coauthors, 2015: The Community Earth System Model (CESM) Large Ensemble Project: A community resource for studying climate change in the presence of internal climate variability. *Bull. Amer. Meteor. Soc.*, 96, 1333– 1349, https://doi.org/10.1175/BAMS-D-13-00255.1.
- Kim, S. T., W. Cai, F.-F. Jin, and J.-Y. Yu, 2014: ENSO stability in coupled climate models and its association with mean state. *Climate Dyn.*, 42, 3313–3321, https://doi.org/10.1007/s00382-013-1833-6.
- Kirtman, B. P., 1997: Oceanic Rossby wave dynamics and the ENSO period in a coupled model. J. Climate, 10, 1690– 1704, https://doi.org/10.1175/1520-0442(1997)010<1690: ORWDAT>2.0.CO;2.
- ——, and P. S. Schopf, 1998: Decadal variability in ENSO predictability and prediction. *J. Climate*, 11, 2804–2822, https://doi.org/ 10.1175/1520-0442(1998)011<2804:DVIEPA>2.0.CO;2.
- Klein, S. A., and D. L. Hartmann, 1993: The seasonal cycle of low stratiform clouds. J. Climate, 6, 1587–1606, https://doi.org/ 10.1175/1520-0442(1993)006<1587:TSCOLS>2.0.CO;2.
- Langen, P. L., R. G. Graversen, and T. Mauritsen, 2012: Separation of contributions from radiative feedbacks to polar amplification on an aquaplanet. *J. Climate*, 25, 3010–3024, https:// doi.org/10.1175/JCLI-D-11-00246.1.
- Larson, S. M., K. V. Pegion, and B. P. Kirtman, 2018: The South Pacific meridional mode as a thermally driven source of ENSO amplitude modulation and uncertainty. *J. Climate*, 31, 5127–5145, https://doi.org/10.1175/JCLI-D-17-0722.1.
- Leith, C., 1973: The standard error of time-averaged estimates of climatic means. *J. Appl. Meteor.*, **12**, 1066–1069, https://doi.org/10.1175/1520-0450(1973)012<1066:TSEOTA>2.0. CO:2.
- Li, L., B. Wang, and G. J. Zhang, 2015: The role of moist processes in shortwave radiative feedback during ENSO in the CMIP5 models. J. Climate, 28, 9892–9908, https://doi.org/10.1175/ JCLI-D-15-0276.1.
- Liu, Z., and H. Yang, 2003: Extratropical control of tropical climate, the atmospheric bridge and oceanic tunnel. *Geophys. Res. Lett.*, 30, 1230, https://doi.org/10.1029/2002gl016492.
- Lloyd, J., E. Guilyardi, H. Weller, and J. Slingo, 2009: The role of atmosphere feedbacks during ENSO in the CMIP3 models. Atmos. Sci. Lett., 10, 170–176, https://doi.org/10.1002/asl.227.
- —, —, and —, 2011: The role of atmosphere feedbacks during ENSO in the CMIP3 models. Part II: Using AMIP runs to understand the heat flux feedback mechanisms. *Climate Dyn.*, 37, 1271–1292, https://doi.org/10.1007/s00382-010-0895-y.
- —, and —, 2012: The role of atmosphere feedbacks during ENSO in the CMIP3 models. Part III: The shortwave flux feedback. *J. Climate*, **25**, 4275–4293, https://doi.org/10.1175/JCLI-D-11-00178.1.
- Loeb, N. G., and Coauthors, 2018: Clouds and the Earth's Radiant Energy System (CERES) Energy Balanced and Filled (EBAF) Top-of-Atmosphere (TOA) edition-4.0 data product. *J. Climate*, **31**, 895–918, https://doi.org/10.1175/JCLI-D-17-0208.1.
- Matei, D., N. Keenlyside, M. Latif, and J. Jungclaus, 2008: Subtropical forcing of tropical Pacific climate and decadal ENSO modulation. *J. Climate*, 21, 4691–4709, https://doi.org/10.1175/2008JCLI2075.1.

- Mauritsen, T., R. G. Graversen, D. Klocke, P. L. Langen, B. Stevens, and L. Tomassini, 2013: Climate feedback efficiency and synergy. *Climate Dyn.*, 41, 2539–2554, https:// doi.org/10.1007/s00382-013-1808-7.
- Myers, T. A., and J. R. Norris, 2015: On the relationships between subtropical clouds and meteorology in observations and CMIP3 and CMIP5 models. *J. Climate*, **28**, 2945–2967, https://doi.org/10.1175/JCLI-D-14-00475.1.
- Neale, R. B., J. H. Richter, and M. Jochum, 2008: The impact of convection on ENSO: From a delayed oscillator to a series of events. *J. Climate*, 21, 5904–5924, https://doi.org/10.1175/ 2008JCLI2244.1.
- Norris, J. R., 1998: Low cloud type over the ocean from surface observations. Part I: Relationship to surface meteorology and the vertical distribution of temperature and moisture. *J. Climate*, **11**, 369–382, https://doi.org/10.1175/1520-0442(1998)011<0369:LCTOTO>2.0.CO:2.
- Okumura, Y. M., and C. Deser, 2010: Asymmetry in the duration of El Niño and La Niña. *J. Climate*, **23**, 5826–5843, https://doi.org/10.1175/2010JCLI3592.1.
- Philander, S. G. H., D. Gu, G. Lambert, T. Li, D. Halpern, N.-C. Lau, and R. C. Pacanowski, 1996: Why the ITCZ is mostly north of the equator. *J. Climate*, 9, 2958–2972, https://doi.org/10.1175/1520-0442(1996)009<2958:WTIIMN>2.0.CO;2.
- Picaut, J., F. Masia, and Y. du Penhoat, 1997: An advective-reflective conceptual model for the oscillatory nature of the ENSO. *Science*, **277**, 663–666, https://doi.org/10.1126/science.277.5326.663.
- Rädel, G., T. Mauritsen, B. Stevens, D. Dommenget, D. Matei, K. Bellomo, and A. Clement, 2016: Amplification of El Niño by cloud longwave coupling to atmospheric circulation. *Nat. Geosci.*, 9, 106–110, https://doi.org/10.1038/ngeo2630.
- Randall, D. A., Harshvardhan, D. A. Dazlich, and T. G. Corsetti, 1989: Interactions among radiation, convection, and largescale dynamics in a general circulation model. *J. Atmos. Sci.*, 46, 1943–1970, https://doi.org/10.1175/1520-0469(1989) 046<1943:IARCAL>2.0.CO;2.
- Schneider, E., B. P. Kirtman, and R. Lindzen, 1999: Tropospheric water vapor and climate sensitivity. J. Atmos. Sci., 56, 1649–1658, https:// doi.org/10.1175/1520-0469(1999)056<1649:TWVACS>2.0.CO;2.
- Slingo, A., and J. M. Slingo, 1988: The response of a general circulation model to cloud longwave radiative forcing. I: Introduction and initial experiments. *Quart. J. Roy. Meteor. Soc.*, 114, 1027–1062, https://doi.org/10.1002/ qj.49711448209.
- Slingo, J. M., and A. Slingo, 1991: The response of a general circulation model to cloud longwave radiative forcing. II: Further studies. *Quart. J. Roy. Meteor. Soc.*, **117**, 333–364, https://doi.org/10.1002/qj.49711749805.
- Soden, B. J., A. J. Broccoli, and R. S. Hemler, 2004: On the use of cloud forcing to estimate cloud feedback. *J. Climate*, 17, 3661–3665, https://doi.org/10.1175/1520-0442(2004)017<3661: OTUOCF>2.0.CO;2.
- Suarez, M. J., and P. S. Schopf, 1988: A delayed action oscillator for ENSO. J. Atmos. Sci., 45, 3283–3287, https://doi.org/10.1175/ 1520-0469(1988)045<3283:ADAOFE>2.0.CO;2.
- Tang, Y., L. Li, W. Dong, and B. Wang, 2016: Tracing the source of ENSO simulation differences to the atmospheric component of two CGCMs. Atmos. Sci. Lett., 17, 155–161, https://doi.org/ 10.1002/asl.637.
- Taylor, K. E., R. J. Stouffer, and G. A. Meehl, 2012: An overview of CMIP5 and the experiment design. *Bull. Amer. Meteor. Soc.*, 93, 485–498, https://doi.org/10.1175/BAMS-D-11-00094.1.

- Trossman, D. S., J. B. Palter, T. M. Merlis, Y. Huang, and Y. Xia, 2016: Large-scale ocean circulation-cloud interactions reduce the pace of transient climate change. *Geophys. Res. Lett.*, **43**, 3935–3943, https://doi.org/10.1002/2016GL067931.
- Voigt, A., and T. A. Shaw, 2015: Circulation response to warming shaped by radiative changes of clouds and water vapour. *Nat. Geosci.*, 8, 102–106, https://doi.org/10.1038/ngeo2345.
- Weisberg, R. H., and C. Wang, 1997: A western Pacific oscillator paradigm for the El Niño–Southern Oscillation. Geophys. Res. Lett., 24, 779–782, https://doi.org/10.1029/97GL00689.
- Wetherald, R. T., and S. Manabe, 1980: Cloud cover and climate sensitivity. *J. Atmos. Sci.*, **37**, 1485–1510, https://doi.org/10.1175/1520-0469(1980)037<1485:CCACS>2.0.CO;2.
- —, and —, 1988: Cloud feedback processes in a general circulation model. *J. Atmos. Sci.*, **45**, 1397–1416, https://doi.org/10.1175/1520-0469(1988)045<1397:CFPIAG>2.0.CO;2.

- Zebiak, S. E., 1985: Tropical atmosphere–ocean interaction and the El Niño/Southern Oscillation phenomenon. Ph.D. thesis, Massachusetts Institute of Technology, 260 pp.
- —, and M. A. Cane, 1987: A model El Niño–Southern Oscillation. *Mon. Wea. Rev.*, **115**, 2262–2278, https://doi.org/10.1175/1520-0493(1987)115<2262:AMENO>2.0.CO;2.
- Zhang, H., A. Clement, and P. Di Nezio, 2014: The South Pacific meridional mode: A mechanism for ENSO-like variability. *J. Climate*, 27, 769–783, https://doi.org/10.1175/JCLI-D-13-00082.1.
- Zhang, M. H., J. J. Hack, J. T. Kiehl, and R. D. Cess, 1994: Diagnostic study of climate feedback processes in atmospheric general circulation models. *J. Geophys. Res.*, 99, 5525–5537, https://doi.org/10.1029/93JD03523.
- Zhang, R., S. M. Kang, and I. M. Held, 2010: Sensitivity of climate change induced by the weakening of the Atlantic meridional overturning circulation to cloud feedback. J. Climate, 23, 378–389, https://doi.org/10.1175/ 2009JCLI3118.1.